Synthesis Factors Dependence of Magnetic Properties of $CoFe_2O_4$ and $CoFe_{2-x}Gd_xO_4$ Semicrystalline Nanoparticles with desired Morphology through Hydrothermal Procedure

Hamid Hosseinzadeh
Hakim Sabzevari University
Hamidreza Oveisi (oveisi@chapman.edu)
Chapman University https://orcid.org/0000-0002-0996-7811

Research Article

Keywords: cobalt ferrite, hydrothermal process, magnetic properties, spherical morphology, semicrystalline, Gd dopant

Posted Date: January 14th, 2022

DOI: https://doi.org/10.21203/rs.3.rs-1240608/v1

Abstract

In the present study, $CoFe_2O_4$ and $CoFe_{2-x}Gd_xO_4$ nanoparticles were synthesized by the hydrothermal process. The $CoFe_2O_4$ nanoparticles were synthesized at different temperatures (70°C, 100°C, 150°C, and 200°C), molar ratio of $CoCl_2$/ $FeCl_3$ (0/2, 0.75/2, 1/2, 1.5/2, and 2/2). Gadolinium-doped cobalt ferrite ($CoFe_{2-x}Gd_xO_4$) nanoparticles have also been synthesized with Gd/Fe molar ratios of 0.18 and 0.53. The XRD patterns indicate that cobalt ferrite and Gadolinium-doped cobalt ferrite nanoparticles have been successfully synthesized without impurities with a medium degree of crystallinity. The XRD patterns show that by increasing the synthesis temperature from 70°C to 200°C, the size of the nanoparticles decreased from 50.49nm to 32.45nm while the morphology of the nanoparticles also changed from a shapeless and agglomerated state to a spherical shape. The XPS curve illustrated several peaks corresponding to Fe^{+3}, Co^{+2}, and O 1s. The binding energies for Co and Fe were consistent with Fe 2p and Co 2p binding energies for cobalt ferrite nanoparticles. The magnetic saturation value (M_s) increased from 17.253 emu/g to 54.438 emu/g with a rise in the synthesis temperature. The effects of $FeCl_3$/$CoCl_2$ molar ratio on the magnetic properties showed the highest value of M_s (54.438 emu/g) and the coercivity (H_C) of 744.56 Oe for a 2/1 molar ratio. The addition of gadolinium to the composition resulted in a reducing of the magnetic properties of nanoparticles; accordingly, the amount of saturated magnetization was reduced to 22.469 emu/g. Another effect of gadolinium dopant in the composition was a change in nanoparticle morphology from spherical to rod shape. The final aim of this study was to investigate the possible utilization of $CoFe_2O_4$ and $CoFe_{2-x}Gd_xO_4$ nanoparticles in medical treatment in the near future.

Summary

•A facile hydrothermal approach for preparation of $CoFe_2O_4$ nanoparticles with spherical morphology

•Study the synthesis temperature, a composition ratio of raw materials, and Gd dopant as three essential parameters on the microstructure and magnetic properties of $CoFe_2O_4$ nanoparticles

•Deeply probe the relationship between the synthesis parameters and dopant concentration on the magnetic saturation and the coercivity values.

•Examining the impact of Gadolinium doping on nanoparticle microstructure, morphology, and magnetic properties.

•Investigate the possible utilization of these nanoparticles for Magnetic Resonance Imaging (MRI) for further research.

1. Introduction

Magnetic nanoparticles are one of the most important and most used types of nanoscale materials which their unique features create specific applications for them compared with other nanostructures[1, 2].

Magnetic nanoparticles are emerging as essential biomedical functional nanomaterials in areas such as drug release, tissue engineering, theranostics, and lab-on-a-chip due to their exclusive chemical and physical properties. Iron oxide-based nanoparticles have wide applications in various fields, such as $ZnFe_2O_4$ nanoparticles in petrochemical[3], nickel ferrite nanocomposites as catalysts, $CoFe_2O_4$ core/shell nanoparticles for advanced hyperthermia application[4], etc. The ease of collecting and retrieving magnetic nanoparticles in their application as a catalyst is one of the advantages of these nanoparticles, which is the reason for their ever-increasing usage in this category[5].

However, the magnetic properties of iron oxide nanoparticles are widely influenced by their physicochemical properties (morphology, size distribution, and surface nature)[6]. On the other hand, the doped element has a great deal of application for iron oxide nanoparticles in various industries, with its favorable magnetic properties.

The formation of the cobalt ferrite phase can be changed the initial properties of iron oxide nanoparticles which can improve the bioapplications of these nanoparticles. Biocompatibility, thermal and chemical stability are the unique properties of spinel ferrite nanoparticles with MFe_2O_4 (M = Cr, Mn, Co, Ni, Cu, and Zn) the general formula, which has led to abundant applications in the diagnosis and medical sciences[4], [5], [7–11]. The crystal structure of $CoFe_2O_4$ is an inverse spinel-type structure where oxygen atoms constitute a face center cubic (FCC) lattice. In this regard, divalent Co^{2+} ions are shifted to octahedral "B" sites, and trivalent Fe^{3+} ions are occupied by both tetrahedral "A" and octahedral "B" sub-lattice sites[7]. This is a good indication that the $CoFe_2O_4$ nanoparticles have been suitable for a wide variety of technological and medical applications[12–15].

There are various synthesis methods for the synthesis of $CoFe_2O_4$ nanoparticles: co-precipitation[8], sol-gel techniques[9, 16], hydrothermal synthesis[10, 17], ultrasonic[18] and thermal decomposition[19, 20]. The $CoFe_2O_4$ nanoparticles are widely used in numerous branches such as catalysts[11], [21–23], food industry[24, 25], electronics[26], and biomedicine[27–30]. The inherent magnetism of these nanoparticles is the most important feature of biomedical applications because of its good compatibility with the human body and the high diagnosis[31].

The substitution of rare-earth cations such as gadolinium into the inverse spinal lattice leads to structural disorder and lattice strain which could bring significant changes in the morphological and magnetic properties. Also, several other parameters can affect the nature of the $CoFe_2O_4$ magnetic nanoparticles. Composition ratio, morphology, degree of crystallinity, particle size distribution, doping, and synthesis temperature influence these materials' magnetic behavior and application. However, the synthesis temperature, dopant, and molar ratio of $FeCl_3$/$CoCl_2$ are the three crucial parameters on the magnetic properties and microstructure of $CoFe_2O_4$ nanoparticles sciences[4], [5, 7, 9, 11].

This study aimed to introduce a possible synthetic pathway for synthesizing semicrystalline cobalt ferrite nanoparticles at low temperatures with the desired morphology. Also, the effects of dopant, hydrothermal

temperature, and the composition ratio of raw materials on the formation and magnetic properties were investigated to achieve the non-agglomerated nanoparticles with spherical morphology and high magnetic saturation value (M_S) value, and low coercivity (H_c).

The paramagnetic properties of iron oxide were considered for use as superparamagnetic nanoparticles in medical applications. It can provide a clear vision in the field of treatment and medical

2. Experimental

2.1 Materials

The raw materials for this study were as follows: $FeCl_3.9H_2O$ by 98% purity, $CoCl_2.6H_2O$ by over 99% purity, $FeCl_2.4H_2O$ by 98% purity, pure gadolinium element (Gd), hydrochloric acid (35%wt), and ultra-pure NaOH, which were prepared from Merck company and were used without any further purification. An aqueous solution of NaOH was used as the alkaline precipitant agent.

2.2 Synthesis of cobalt ferrite ($CoFe_2O_4$)

The $CoFe_2O_4$ nanoparticles were synthesized by a hydrothermal process at different temperatures (70^oC, 100^oC, 150^oC, and 200^oC). The molar ratio of $CoCl_2$/ $FeCl_3$: 0/2, 0.75/2, 1/2, 1.5/2, and 2/2 were used to synthesize nanoparticles with different types of magnetic properties and morphologies. At first, $FeCl_3.9H_2O$ and $CoCl_2.6H_2O$ were dissolved in 100ml distilled water under vigorous stirring with a constant speed for 40 min to homogenize the solution. Then the pH was adjusted to 10 by adding drop by drop NaOH solution. The final solution was transferred into a 150ml Teflon-lined stainless-steel autoclave, sealed, and kept in the oven for 16h. The black precipitates were collected and washed several times with distilled water and ethanol. Finally, nanoparticles were dried in the oven at 50^oC for 3h. The sample names and different synthesis parameters are listed in table1.

2-3- Synthesis of Gd doped cobalt ferrite ($CoFe_{2-x}\ Gd_xO_4$) nanoparticles

The stoichiometric amounts of $FeCl_3.9H_2O$ and $CoCl_2.6H_2O$ were dissolved in 100ml distilled water and stirred for 15 minutes at room temperature. Afterward, a specific quantity of gadolinium was dissolved in 3ml hydrochloric acid (35%wt) to dissolve pure gadolinium. Upon dissolution of gadolinium, the gadolinium solution was added to the initial solution and stirred for an additional 30 minutes. The atomic ratios of gadolinium (x) doped in the composition were X: 0.00, 0.30, and 0.70. Reducing the amount of gadolinium chloride ($GdCl_3$) from the amount of iron chloride will ensure that the ratio of iron chloride and cobalt chloride remains constant at 2:1. NaOH solution was added drop-by-drop into the final solution until the pH was adjusted to 10. At last, a solution was placed in a 150 ml Teflon-lined stainless

steel autoclave, sealed, and kept at 200°C for 16 hours. The black precipitates were collected and washed several times with distilled water and ethanol and dried in the oven at 50^{o}C for 3h.

2.4 Materials characterization

The X-ray diffraction (XRD) patterns of the particles were collected on a Philips X'pert pw3040/60 X-ray diffractometer with Cu kα radiation (λ = 0.15147nm). Field emission scanning electron microscope (FESEM) images and energy-dispersive X-ray spectroscopy (EDS) were obtained by Tescan BRONO-mira3 LMU. A magnetic hysteresis loop of samples was measured at room temperature using a vibrating sample magnetometer (VSM) model 7407 Lakeshore cryotronics. X-ray photoelectron spectroscopy (XPS) was performed at room temperature using a JPS-9010TR (JEOL) instrument with an Mg Kα X-ray source. All binding energies were calibrated by referencing C 1s (285.0 eV).

3. Results And Discussion

3.1 Phase and morphology identification

The XRD patterns of the samples synthesized at different hydrothermal temperatures (Fig. 1a) and different molar ratios of $CoCl_2$/$FeCl_3$ (Fig. 1b) are shown in Fig. 1. The XRD patterns indicate that cobalt ferrite nanoparticles have been successfully synthesized without unwanted and extra phases and impurities. Seven characteristic peaks could be indexed as a cubic structure of semicrystalline $CoFe_2O_4$ nanoparticles. The lattice parameter was a=0.8379nm, corresponding to the JCPDS card no.02-1045. Given that the value of the obtained lattice parameter is close to its theoretical value ($\approx$ 0.8402nm)[32], it could be concluded that nanoparticles have a medium degree of crystallinity.

Figure 1b shows the diffraction peaks of Fe_2O_3 and Fe_3O_4 as impurity phases in the CFN 6 sample due to the imbalanced stoichiometric ratios of Co^{+2} and Fe^{+3} ions[33]. By increasing the amount of cobalt to iron molar ratio (CFN 4), the unwanted phases of Fe_2O_3 and Fe_3O_4 were eliminated. Two XRD peaks were observed at 58.615^{o} and 64.402^{o} for the CFN 8 sample, assigning to the cobalt oxide (Co_3O_4) crystal phase. The average crystallite size of nanoparticles was calculated by the Scherer equation (D_{hkl}=Kλ/ ßcosθ), where D_{hkl} is the crystallite size derived from the (400) peaks of the XRD patterns, k the sphere shape factor (0.89), θ the angle of the diffraction, ß the full-width at half-maximum (FWHM) of the (400) peak of the sample.

The data in Table 2 illustrates that an increase of synthesis temperature from 70°C to 200°C leads to a decrease in the crystallite size from 50.49nm to 32.45nm. These results also can be confirmed with the obtained particle size by FESEM. Increasing the hydrothermal synthesis temperature may enhance the nanostructure properties, especially for $CoFe_2O_4$ nanoparticles. The bonds will be broken, and the order through the $CoFe_2O_4$ nanoparticles will be increased, and consequently, the crystallite size will be decreased. With increasing the hydrothermal temperature, the $CoFe_2O_4$ crystallites nucleates and grow,

the boundaries between crystallites at which amorphous transforms to crystals decrease in volume. This reduction limits the nucleation and growth of the crystalline phase, as seen in the XRD patterns[34].

Also, by increasing the hydrothermal temperature over 100°C, the degree of crystallinity increased up to 28%. The highest degree of crystallinity was achieved for CFN 1 sample. The crystallite size was changed from 31.64nm to 37.85nm for CFN 4 and CFN 7 samples by enhancing of $CoCl_2$ content in the reaction medium.

According to X-ray diffraction patterns in Fig. 1c, it becomes clear that by increasing the Gd dopant amount to x = 0.30, the intensity of the peaks increased. Some peaks appeared at 30.9, 286.36, 185.33, 199.49, and 288.60 degrees related to gadolinium oxide (Gd_2O_3), according to the reference data (JCPDS card no.01-0339). When the dopant value was increased to x= 0.70, the peaks intensity increased once more, and new peaks appeared. A sharp decrease in crystal size was observed by adding gadolinium atoms to the $CoFe_2O_4$ compound (x=0.30 and x=0.70), and the degree of crystallinity decreased from 40.585 to 33.902% due to changes in the morphology and crystal structure of the nanoparticles[35].

The FESEM images of nanoparticles are shown in Fig. 2, Fig. 3, and Fig. 4. The pictures show the effect of hydrothermal temperature on the size and morphology of nanoparticles. As illustrated in the images, increasing the synthesis temperature resulted in a decrease in the size of the nanoparticles. On the other hand, by increasing the cobalt amount in the composition, nanoparticles and agglomeration size increased, which are presented in Table 2. The nanoparticles with irregular morphology and agglomerated state at 70^oC changed to spherical shape at 200^oC. By increasing the synthesis temperature, the uniform size distribution of the nanoparticles was raised, and the agglomeration of the particles was reduced. It is specified that increasing the cobalt molar ratio in the hydrothermal medium can increase the agglomeration of the particles in the final products[17]. In Figure 4, the effect of the Gd dopant on the size and morphology of nanoparticles is visible, as, in x = 0.30 dopant amount of Gd, the morphology of the nanoparticles changed from 100% quasi-spherical shape to a mixture of quasi-spherical and rod shape. Semi-spherical nanoparticles with an approximate size of 20 to 30 nm and rod shape nanoparticles with a thickness of 20 to 35 nm and length of 200 to 550 nm were estimated. In the $CFNG_{0.70}$ sample, the morphology of nanoparticles was changed entirely to the unique rod shape. The reason for the nanoparticles' morphology changes is the strong distortion of the crystal lattice and change in the preferential growth directions due to the presence of gadolinium atoms in the crystal structure of nanoparticles[36, 37].

The EDS elemental map of CFN 4 and $CFNG_{0.30}$ magnetic nanoparticles is shown in Fig. 5 and Fig. 6. The images and results of the EDS elemental map clearly show the uniform intensity of Fe, Co, Gd, and O signals resulting from a uniform distribution of the elements. There was no trace of element segregation and aggregation in the microstructure of the nanoparticles.

The chemical composition of $CoFe_2O_4$ nanoparticles synthesized at 200^oC (CFN 4) was further investigated by XPS. The XPS peaks of Co, Fe, and O elements can be seen in Fig. 5. The binding energy

of the C 1s peak at 285.0 eV was used as a reference for calibration.

The corresponding spectroscopy curve and the concentration table of the existing elements are shown in Fig. 7 and Table.4. The peaks at 709.6 ev, 711.1 eV, and 712.0 eV correspond to Fe^{+3}, and the peaks at 778.5 eV and 780.4 eV were assigned to Co^{+2}. The peak located at 529.9 eV is attributed to the O 1s region. These binding energies for Co and Fe are consistent with Fe 2p and Co 2p binding energies for cobalt ferrite nanoparticles[38]. Also, some small XPS peaks indicate negligible amounts of Ca, Na, and Cl elements as impurities.

3.2 Determination of magnetic properties

Figure 8 and Table.5 show the magnetization value versus the magnetic field at room temperature. In Figure 8.a, the hysteresis loops of the samples synthesized at different temperatures are shown. By increasing the synthesis temperature, nanoparticles' magnetization was increased in large quantities so that the magnetic saturation value (M_s) increased from 17.253 emu/g to 54.438 emu/g for CFN1 and CFN4 samples, respectively.

The coercivity field, Hc, can reflect the ferromagnetism or ferrimagnetism properties. This value describes the force that is necessary to demagnetize a sample completely. By increasing the synthesis temperature, the value of coercivity (Hc) was reduced from 1648.2 Oe at 70°C to 398.83 Oe at 200°C, while the value of retentivity (Mr) was enhanced from 8.360emu/g to 18.245emu/g. The obtained value of H_c for the CFN 4 sample (398.83Oe) is much lower than the reported value by Demortière et al.[39]. Increasing the synthesis temperature, resulting in smaller crystallites and improved crystallinity, a considerable rise in magnetic saturation, and a drop in coercivity and retentivity values could be achieved by increasing the synthesis temperature [40].

The hysteresis loops of the samples synthesized by different combination ratios are shown in Fig. 8b. As the results show, the highest value of magnetic saturation (M_S) is related to the CFN 4 sample with a 1/2 molar ratio. The magnetic saturation value decreases impressively by increasing the cobalt amount in CFN 7 and CFN 8 samples. The CFN 6 sample has less magnetization saturation compared to CFN 4 sample, while it's higher than the value obtained for the CFN 7 and CFN 8 samples. The lowest and highest values of coercivity (H_c) were obtained for CFN 8 (95.28 Oe) and CFN 6 (744.56 Oe) samples, respectively. The excess amount of cobalt in the hydrothermal medium can persuade the formation of the Co_3O_4 compound in CFN 7 and CFN 8 samples, affecting the obtained value of magnetic saturation. The sharp decrease in magnetic saturation was observed by increasing the molar ratio of $CoCl_2$/ $FeCl_3$ from 1/2 to 1.5/2 and 1/1[41].

The hysteresis loops of the samples with different amounts of Gd dopant and changes in the magnetic properties are shown in Fig. 8c. $CoFe_2O_4$ nanoparticles (CFN 4) showed the highest value of magnetic saturation on a measuring scale of 54.4381 emu/g. In this experiment, the magnetic properties of the nanoparticles were drastically reduced by adding gadolinium so that the value of M_S was reduced to

22.947(emu/g) in $CFNG_{0.70}$. The value of H_c increased from 22.947(Oe) to 1358.800(Oe), which the reason could be the onset of morphological changes from quasi-spherical to rod shape, an increase of nanoparticles size, and the possible presence of gadolinium oxide in the composition[37].

Inbaraj et al.[42] have synthesized the cobalt ferrite nanoparticles by hydrothermal method at 180°C for 24h. The M_s value of their synthesized nanoparticles was 35 emu/g which had fewer magnetic properties than CFN3 and CFN4 samples (36.136 emu/g and 54.438 emu/g) synthesized at lower temperature and shorter time (150°C and 200°C for 16h) in the present study.

4. Conclusions

$CoFe_2O_4$ nanoparticles with spherical morphology were synthesized by the hydrothermal process at low temperatures. The results clearly showed that by increasing the synthesis temperature, the size of nanoparticles was changed in the range of 50.49nm to 32.45nm, and the morphology of nanoparticles changed from irregular morphology and agglomerated state at 70°C to semi-spherical shape at 200°C. The magnetic saturation increased from 17.253emu/g to 54.438emu/g by increasing the synthesis temperature from 70°C to 200°C. The most suitable combination ratio for the highest magnetic saturation was $CoCl_2$/$FeCl_3$:1/2, in which the entire phase structure was composed entirely of cobalt ferrite spinel, and there was no trace of impurities. The results of different combination ratios determined that the effect of the presence of cobalt oxide (Co_3O_4) on the reduction of magnetic properties of synthesized nanoparticles was more than iron oxide phases (Fe_2O_3, Fe_3O_4). Accordingly, it can be concluded that cobalt ferrite nanoparticles synthesized at 200°C with a composition ratio of $CoCl_2$/$FeCl_3$:1/2 has nanometer size, regular spherical morphology, and higher superparamagnetic property. Finally, the results of Gadolinium dopant showed a sharp decrease in magnetic properties and changes in the morphology of nanoparticles from quasi-spherical to rod shape, which these changed shape nanoparticles by Considering their dimensions and magnetic properties can be used in various fields[43–45].

Declarations

Funding: N/A

Conflicts of interest/Competing interests: The authors certify that they have NO affiliations with or involvement in any organization or entity with any financial interest or non-financial interest in the subject matter or materials discussed in this manuscript.)

Availability of data and material: The raw/processed data required to reproduce these findings can be shared upon request.

Code availability: N/A

Authors' contributions: N/A

Ethics approval: N/A

Consent to participate: N/A

Consent for publication: N/A

References

1. A. Manikandan, R. Sridhar, S.A. Antony, S. Ramakrishna, A simple aloe vera plant-extracted microwave and conventional combustion synthesis: morphological, optical, magnetic and catalytic properties of CoFe2O4 nanostructures. J. Mol. Struct. **1076**, 188–200 (2014)
2. G. Gao et al., Shape-Controlled Synthesis and Magnetic Properties of Monodisperse Fe_3O_4 Nanocubes. Cryst. Growth Des. **10**(7), 2888–2894 (2010). doi:10.1021/cg900920q
3. N.M. Mahmoodi, M. Bashiri, S.J. Moeen, Synthesis of nickel – zinc ferrite magnetic nanoparticle and dye degradation using photocatalytic ozonation. Mater. Res. Bull. **47**(12), 4403–4408 (2012). doi:10.1016/j.materresbull.2012.09.036
4. A. Sunny et al., Magnetic properties of biocompatible CoFe2O4 nanoparticles using a facile synthesis. Nano-Structures \& Nano-Objects **16**, 69–76 (2018)
5. K.K. Senapati, C. Borgohain, P. Phukan, Synthesis of highly stable CoFe2O4 nanoparticles and their use as magnetically separable catalyst for Knoevenagel reaction in aqueous medium. J. Mol. Catal. A Chem. **339**(1–2), 24–31 (2011)
6. D.L. Huber, Synthesis, properties, and applications of iron nanoparticles. Small **1**(5), 482–501 (2005). doi:10.1002/smll.200500006
7. P. Roy, S.M. Hoque, S.I. Liba, S. Choudhury, Investigation of various magnetic features of spinel type cobalt ferrite (CoFe2O4) nanoparticles tuned by annealing temperature. AIP Adv. **8**(10), 105124 (2018)
8. Y. Qu, H. Yang, N. Yang, Y. Fan, H. Zhu, G. Zou, The effect of reaction temperature on the particle size, structure and magnetic properties of coprecipitated CoFe2O4 nanoparticles. Mater. Lett. **60**, no. 29–30 (2006), “,”, , pp. 3548–3552
9. M. Gharibshahian, M. S. Nourbakhsh, and O. Mirzaee, “Evaluation of the superparamagnetic and biological properties of microwave assisted synthesized Zn & Cd doped CoFe2O4 nanoparticles via Pechini sol–gel method,” *J. Sol-Gel Sci. Technol.*, vol. 85, no. 3, pp. 684–692, 2018, doi: 10.1007/s10971-017-4570-1.
10. Q. Liu, J. Sun, H. Long, X. Sun, X. Zhong, and Z. Xu, “Hydrothermal synthesis of CoFe2O4 nanoplatelets and nanoparticles,” *Mater. Chem. Phys.*, vol. 108, no. 2–3, pp. 269–273, 2008.
11. M.M. Dutta, P. Phukan, Cu-doped CoFe2O4 nanoparticles as magnetically recoverable catalyst for CN cross-coupling reaction. Catal. Commun. **109**, 38–42 (2018)

12. H. Oveisi et al., Unusual antibacterial property of mesoporous titania films: Drastic improvement by controlling surface area and crystallinity. Chem. - An Asian J. **5**(9), 1978–1983 (2010). doi:10.1002/asia.201000351
13. E. Sistanipour, A. Meshkini, H. Oveisi, Catechin-conjugated mesoporous hydroxyapatite nanoparticle: A novel nano-antioxidant with enhanced osteogenic property. Colloids Surfaces B Biointerfaces **169**, 329–339 (2018). doi:10.1016/j.colsurfb.2018.05.046
14. J. Robles, R. Das, M. Glassell, M.-H. Phan, H. Srikanth, Exchange-coupled Fe3O4/CoFe2O4 nanoparticles for advanced magnetic hyperthermia. AIP Adv. **8**(5), 56719 (2018)
15. F. Jalali, H. Oveisi, A. Meshkini, Enhanced osteogenesis properties of titanium implant materials by highly uniform mesoporous thin films of hydroxyapatite and titania intermediate layer. J. Mater. Sci. Mater. Med. **31**(12), 1–15 (2020). doi:10.1007/s10856-020-06450-1
16. Y. Lu, Y. Yin, B.T. Mayers, Y. Xia, Modifying the Surface Properties of Superparamagnetic Iron Oxide Nanoparticles through a Sol-Gel Approach. Nano Lett. **2**(3), 183–186 (2002). doi:10.1021/nl015681q
17. D. Zhao, X. Wu, H. Guan, E. Han, Study on supercritical hydrothermal synthesis of CoFe2O4 nanoparticles. J. Supercrit. Fluids **42**(2), 226–233 (2007)
18. Z. Mo, C. Zhang, R. Guo, S. Meng, J. Zhang, Synthesis of Fe3O4 nanoparticles using controlled ammonia vapor diffusion under ultrasonic irradiation. Ind. \& Eng. Chem. Res. **50**(6), 3534–3539 (2011)
19. S. Bela\"\id, D. Stanicki, L. Vander Elst, R.N. Muller, S. Laurent, Influence of experimental parameters on iron oxide nanoparticle properties synthesized by thermal decomposition: size and nuclear magnetic resonance studies. Nanotechnology **29**(16), 165603 (2018)
20. P. Guardia, A. Labarta, X. Batlle, “Tuning the Size, the Shape, and the Magnetic Properties of Iron Oxide Nanoparticles,” *J. Phys. Chem. C*, pp. 390–396, 2011
21. M. Chandel, B.K. Ghosh, D. Moitra, M.K. Patra, S.R. Vadera, N.N. Ghosh, Synthesis of Various Ferrite (MFe2O4) Nanoparticles and Their Application as Efficient and Magnetically Separable Catalyst for Biginelli Reaction. J. Nanosci. Nanotechnol. **18**(4), 2481–2492 (2018)
22. R.M. Borade, P.R. Shinde, S.B. Kale, R.P. Pawar, “Preparation, characterization and catalytic application of CoFe2O4 nanoparticles in the synthesis of benzimidazoles,” in *AIP Conference Proceedings*, 2018, vol. 1953, p. 030194, doi: 10.1063/1.5032529
23. M. Cao et al., Food related applications of magnetic iron oxide nanoparticles: Enzyme immobilization, protein purification, and food analysis. Trends Food Sci. Technol. **27**(1), 47–56 (2012). doi:10.1016/j.tifs.2012.04.003
24. S. Neethirajan, D.S. Jayas, Nanotechnology for the Food and Bioprocessing Industries. Food Bioprocess Technol. **4**(1), 39–47 (2011). doi:10.1007/s11947-010-0328-2
25. N. Matinise et al., Green synthesis of novel zinc iron oxide (ZnFe2O4) nanocomposite via Moringa Oleifera natural extract for electrochemical applications. Appl. Surf. Sci. **446**, 66–73 (2018). doi:10.1016/j.apsusc.2018.02.187

26. H. Fatima, K.-S. Kim, “Iron-based magnetic nanoparticles for magnetic resonance imaging,” *Adv. Powder Technol.*, vol. 29, no. 11, pp. 2678–2685, Nov. 2018, doi: 10.1016/j.apt.2018.07.017
27. Y.B. Lv et al., Magnetic resonance imaging quantification and biodistribution of magnetic nanoparticles using: T 1-enhanced contrast. J. Mater. Chem. B **6**(10), 1470–1478 (2018). doi:10.1039/c7tb03129g
28. E.D. Smolensky, H.Y.E. Park, T.S. Berquó, V.C. Pierre, Surface functionalization of magnetic iron oxide nanoparticles for MRI applications - effect of anchoring group and ligand exchange protocol. Contrast Media Mol. Imaging **6**(4), 189–199 (2011). doi:10.1002/cmmi.417
29. B. Bittova, J. Poltierova-Vejpravova, A.G. Roca, M.P. Morales, V. Tyrpekl, Effects of coating on magnetic properties in iron oxide nanoparticles. J. Phys. Conf. *Ser.* **200**(7), 072012 (Jan. 2010). doi:10.1088/1742-6596/200/7/072012
30. A.S. Teja, P.-Y. Koh, Synthesis, properties, and applications of magnetic iron oxide nanoparticles. Prog. Cryst. growth Charact. Mater. **55**, no. 1–2 (2009), “,”, , pp. 22–45
31. H. Kratz et al., “Novel magnetic multicore nanoparticles designed for MPI and other biomedical applications: From synthesis to first in vivo studies,” *PLoS One*, vol. 13, no. 1, p. e0190214, Jan. 2018, doi: 10.1371/journal.pone.0190214
32. I. Sharifi, H. Shokrollahi, M.M. Doroodmand, R. Safi, Magnetic and structural studies on CoFe2O4 nanoparticles synthesized by co-precipitation, normal micelles and reverse micelles methods. J. Magn. Magn. Mater. **324**(10), 1854–1861 (2012)
33. T.A.S. Ferreira, J.C. Waerenborgh, M. Mendonça, M.R. Nunes, F.M. Costa, Structural and morphological characterization of FeCo2O4 and CoFe2O4 spinels prepared by a coprecipitation method. Solid State Sci. **5**(2), 383–392 (2003)
34. Z.S. Khalifa, Grain size reduction on nanostructured TiO 2 thin films due to annealing. RSC Adv. **7**(48), 30295–30302 (2017)
35. G. Kasi, J. Seo, Influence of Mg doping on the structural, morphological, optical, thermal, and visible-light responsive antibacterial properties of ZnO nanoparticles synthesized via co-precipitation. Mater. Sci. Eng. C **98**, 717–725 (2019)
36. R.V. Yadav, R.K. Verma, G. Kaur, S.B. Rai, Change in structural morphology on addition of ZnO and its effect on fluorescence of Yb3+/Er3+ doped Y2O3. Spectrochim. Acta Part A Mol. Biomol. Spectrosc. **103**, 216–221 (2013)
37. J.Y. Park et al., Paramagnetic ultrasmall gadolinium oxide nanoparticles as advanced T 1 MRI contrast agent: account for large longitudinal relaxivity, optimal particle diameter, and in vivo T 1 MR images. ACS Nano **3**(11), 3663–3669 (2009)
38. W. WP, H. Yang, T. Xian, J. JL, XPS and magnetic properties of CoFe2O4 nanoparticles synthesized by a polyacrylamide gel route. Mater. Trans. **53**(9), 1586–1589 (2012)
39. A. Demortiere et al., Size-dependent properties of magnetic iron oxide nanocrystals. Nanoscale **3**(1), 225–232 (2011)

40. Z. Zi, Y. Sun, X. Zhu, Z. Yang, J. Dai, W. Song, Synthesis and magnetic properties of CoFe2O4 ferrite nanoparticles. J. Magn. Magn. Mater. **321**(9), 1251–1255 (2009)
41. S. Farhadi, J. Safabakhsh, P. Zaringhadam, “Synthesis, characterization, and investigation of optical and magnetic properties of cobalt oxide (Co 3 O 4) nanoparticles,” vol. 3, no. 69, pp. 1–9, 2013, doi: 10.1186/2193-8865-3-69
42. D.J. Inbaraj, B. Chandran, C. Mangalaraj, Synthesis of CoFe2O4 and CoFe2O4/g-C3N4 nanocomposite via honey mediated sol-gel auto combustion method and hydrothermal method with enhanced photocatalytic and efficient Pb+ 2 adsorption property. Mater. Res. Express **6**(5), 55501 (2019)
43. B. Karagoz et al., An efficient and highly versatile synthetic route to prepare iron oxide nanoparticles/nanocomposites with tunable morphologies. Langmuir **30**(34), 10493–10502 (2014). doi:10.1021/la502656u
44. S. Gil, C.R. Correia, J.F. Mano, Magnetically labeled cells with surface-modified Fe3O4 spherical and rod-shaped magnetic nanoparticles for tissue engineering applications. Adv. Healthc. Mater. **4**(6), 883–891 (2015). doi:10.1002/adhm.201400611
45. A. Maleki, P. Zand, Z. Mohseni, Fe3O4@PEG-SO3H rod-like morphology along with the spherical nanoparticles: Novel green nanocomposite design, preparation, characterization and catalytic application. RSC Adv. **6**(112), 110928–110934 (2016). doi:10.1039/c6ra24029a

Tables

Table.1. Sample names and synthesis parameters of cobalt ferrite ($CoFe_2O_4$) nanoparticles

Sample name	Synthesis temperature (°C)	$CoCl_2$/ $FeCl_3$ molar ratio	$FeCl_2$/$FeCl_3$ molar ratio	Gd dopant (Gd/Fe molar ratio)	Reaction atmosphere
CFN 1	70	1/2	-	0.00	Air
CFN 2	100	1/2	-	0.00	Air
CFN 3	150	1/2	-	0.00	Air
CFN 4	200	1/2	-	0.00	Air
CFN 5	200	0/2	1/2	0.00	Nitrogen
CFN 6	200	0.75/2	-	0.00	Air
CFN 7	200	1.5/2	-	0.00	Air
CFN 8	200	2/2	-	0.00	Air
$CFNG_{0.30}$	200	1/2	-	0.18	Air
$CFNG_{0.70}$	200	1/2	-	0.53	Air

Table.2 Textural parameters of $CoFe_2O_4$ nanoparticles with different synthesis conditions

Sample name	FWHM	$d_{(400)}$-spacing (Å)	Degree of crystallinity (%)	Crystallite size (±2nm)	Nanoparticles size (±3nm)	Lattice constant(Å)
CFN 1	0.177	2.07	31.95	50	42	8.29
CFN 2	0.236	2.08	17.81	37	32	8.33
CFN 3	0.236	2.08	25.84	37	29	8.32
CFN 4	0.275	2.07	27.92	31	28	8.30
CFN 5	0.275	2.07	26.81	32	35	8.29
CFN 6	0.275	2.07	28.53	32	28	8.30
CFN 7	0.236	2.07	26.17	37	33	8.30
CFN 8	0.354	2.07	29.96	25	30	8.29

Table.3 Textural parameters of $CoFe_{2-x}Gd_xO_4$ nanoparticles with different amounts of Gd dopant

Dopant amount	FWHM	$d_{(400)}$-spacing (Å)	Degree of crystallinity (%)	Crystallite size(nm)	Lattice constant (Å)
CFN4	0.275	2.075	27.920	32.45	8.30
$CFNG_{0.30}$	0.393	2.074	40.585	22.72	8.29
$CFNG_{0.70}$	0.314	2.071	33.902	28.40	8.28

Table.4. Atomic concentrations of CFN 4 nanoparticles (calculated using the survey spectra)

C1s	O1s	Na1s	Cl2p	Ca2p	Fe2p	Co2p
20.2%	48.2%	0.5%	0.4%	0.9%	19.7%	10.1%
Fe:Co=1.95:1.00						

Table.5. Magnetic properties of the nanoparticles synthesized at different temperatures

Sample name	Magnetization (M_s) emu/g	Coercivity (H_c) Oe	Retentivity (M_r) emu/g
CFN 1	17.25	1648.20	8.36
CFN 2	22.71	1413.00	10.18
CFN 3	36.13	639.49	12.07
CFN 4	54.43	398.83	18.24
CFN 5	29.22	48.45	0.72
CFN 6	52.71	744.56	11.42
CFN 7	39.24	578.13	12.30
CFN 8	34.60	95.27	2.47
$CFNG_{0.30}$	25.312	879.280	10.053
$CFNG_{0.70}$	22.469	1358.800	10.704

Figures

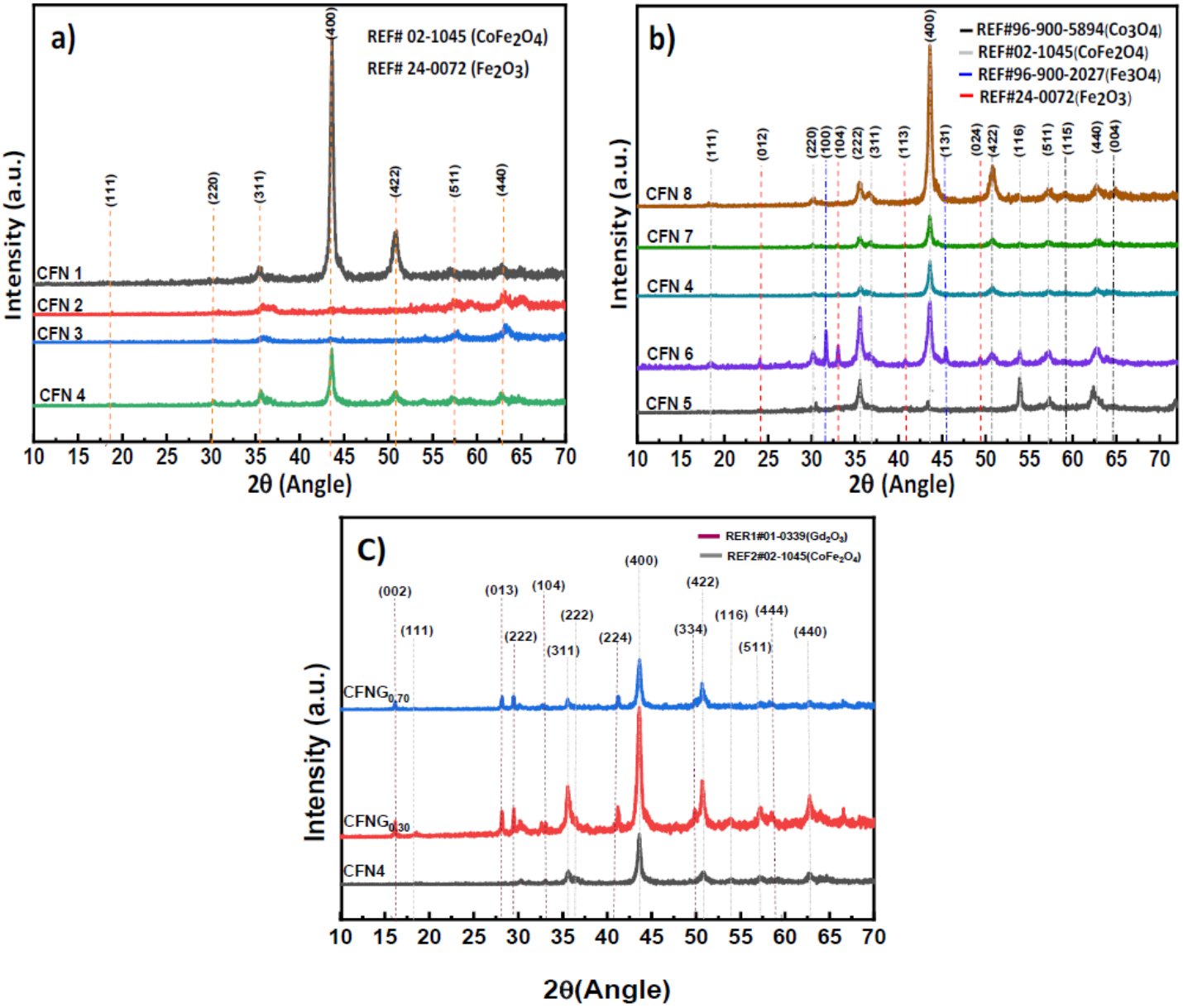

Figure 1

XRD patterns of $CoFe_2O_4$ nanoparticles synthesized at different synthesis temperatures (a), $CoFe_2O_4$ nanoparticles synthesized with varying ratios of composition (b), and Gd doped cobalt ferrite nanoparticles ($CoFe_{2-x}Gd_xO_4$) (c)

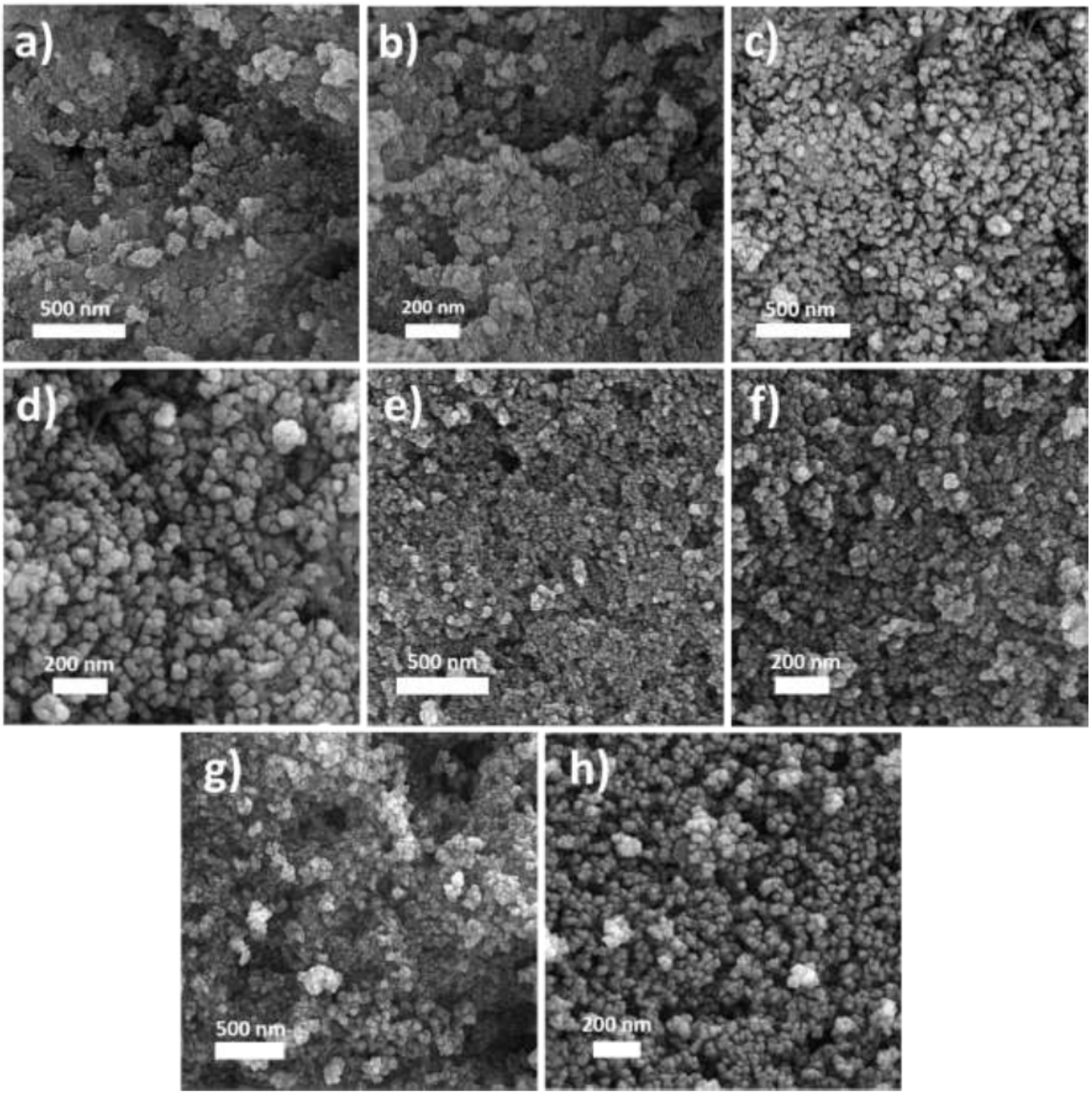

Figure 2

FESEM images of $CoFe_2O_4$ nanoparticles synthesized at different synthesis temperatures. (a, b): CFN 1; (c, d): CFN 2; (e, f): CFN 3; (g, h): CFN 4

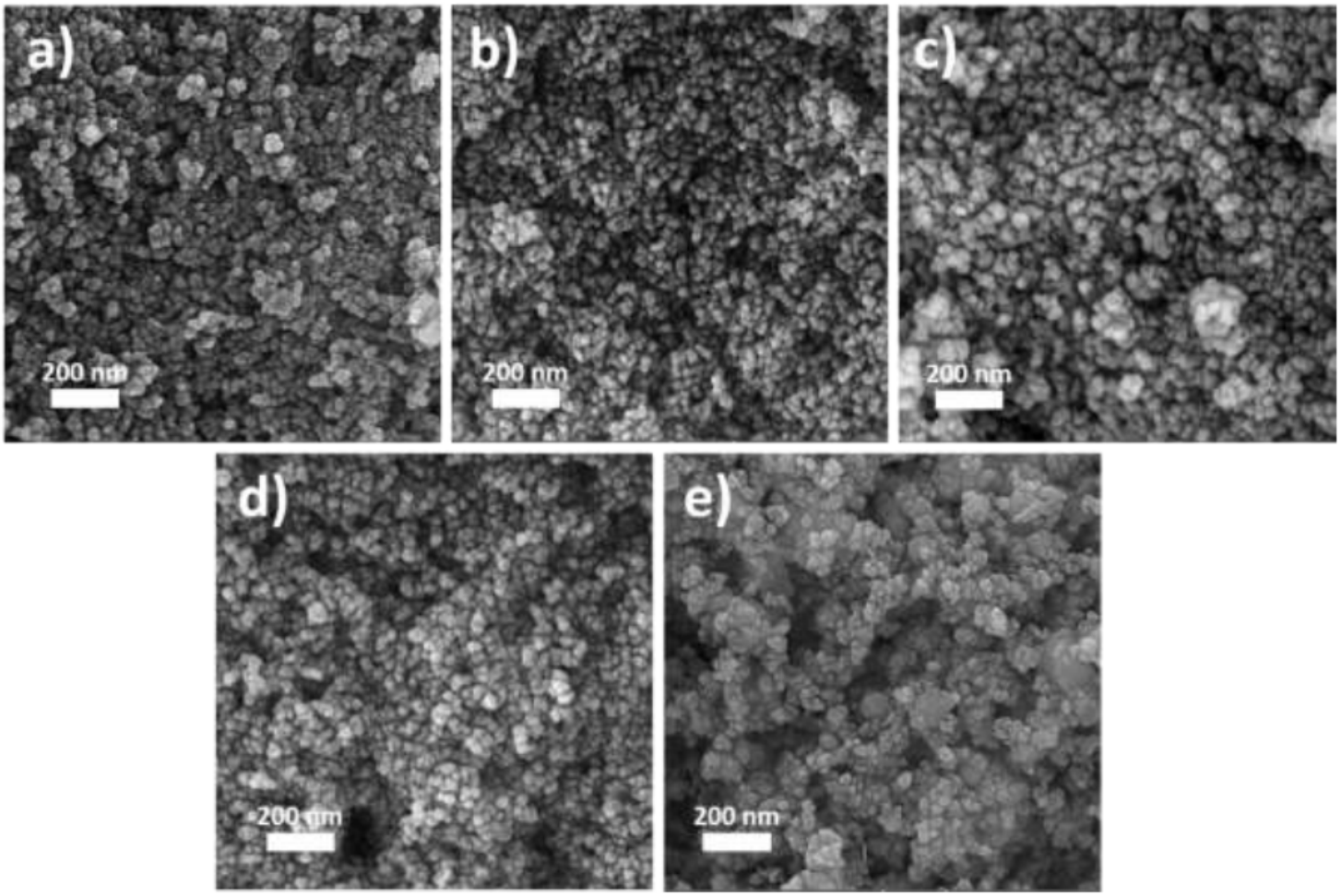

Figure 3

FESEM images of $CoFe_2O_4$ nanoparticles synthesized with different composition ratios. (a): CFN 5; (b): CFN 6; (c): CFN 4; (d): CFN 7; (e): CFN 8

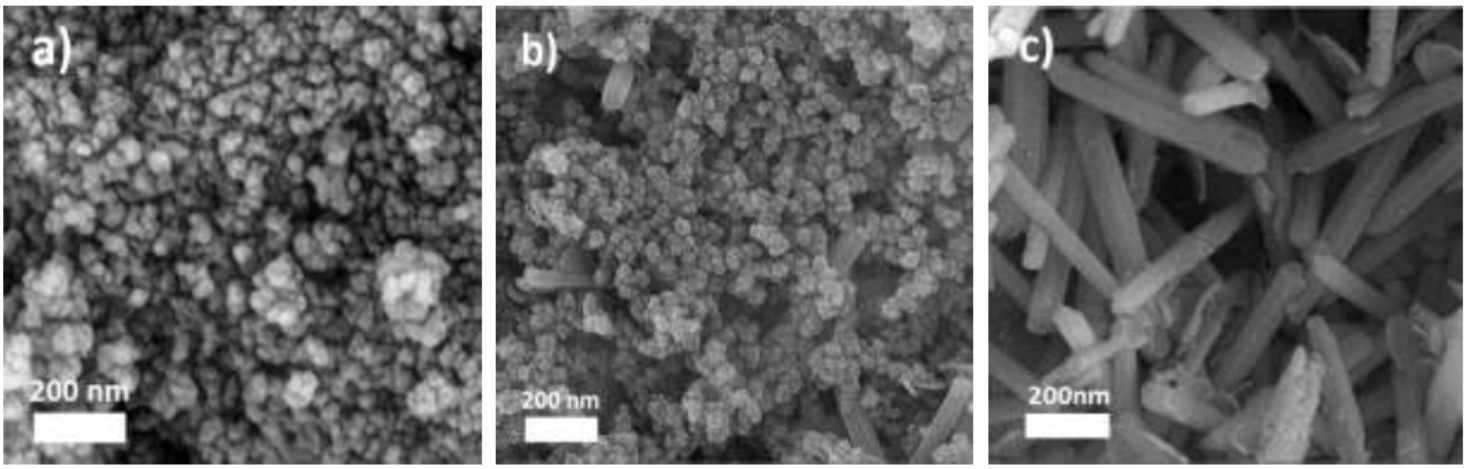

Figure 4

FESEM images of $CoFe_{2-}xGd_xO_4$ nanoparticles doped by different amounts of Gd. (a): CFN4; (b): $CFNG_{0.30}$; (c): $CFNG_{0.70}$

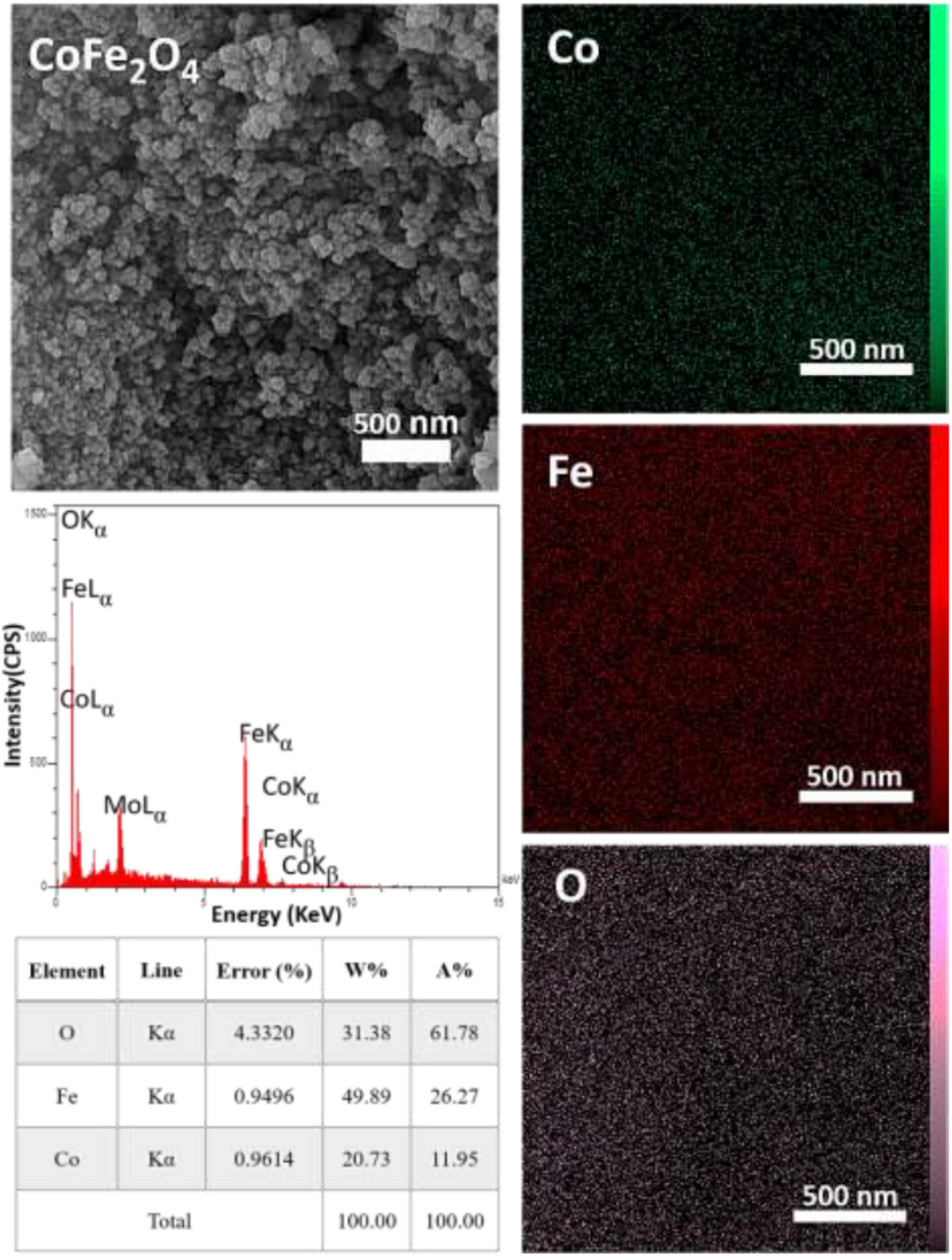

Element	Line	Error (%)	W%	A%
O	Kα	4.3320	31.38	61.78
Fe	Kα	0.9496	49.89	26.27
Co	Kα	0.9614	20.73	11.95
Total			100.00	100.00

Figure 5

FESEM image, EDS pattern, and elemental map of CFN 4 magnetic nanoparticles

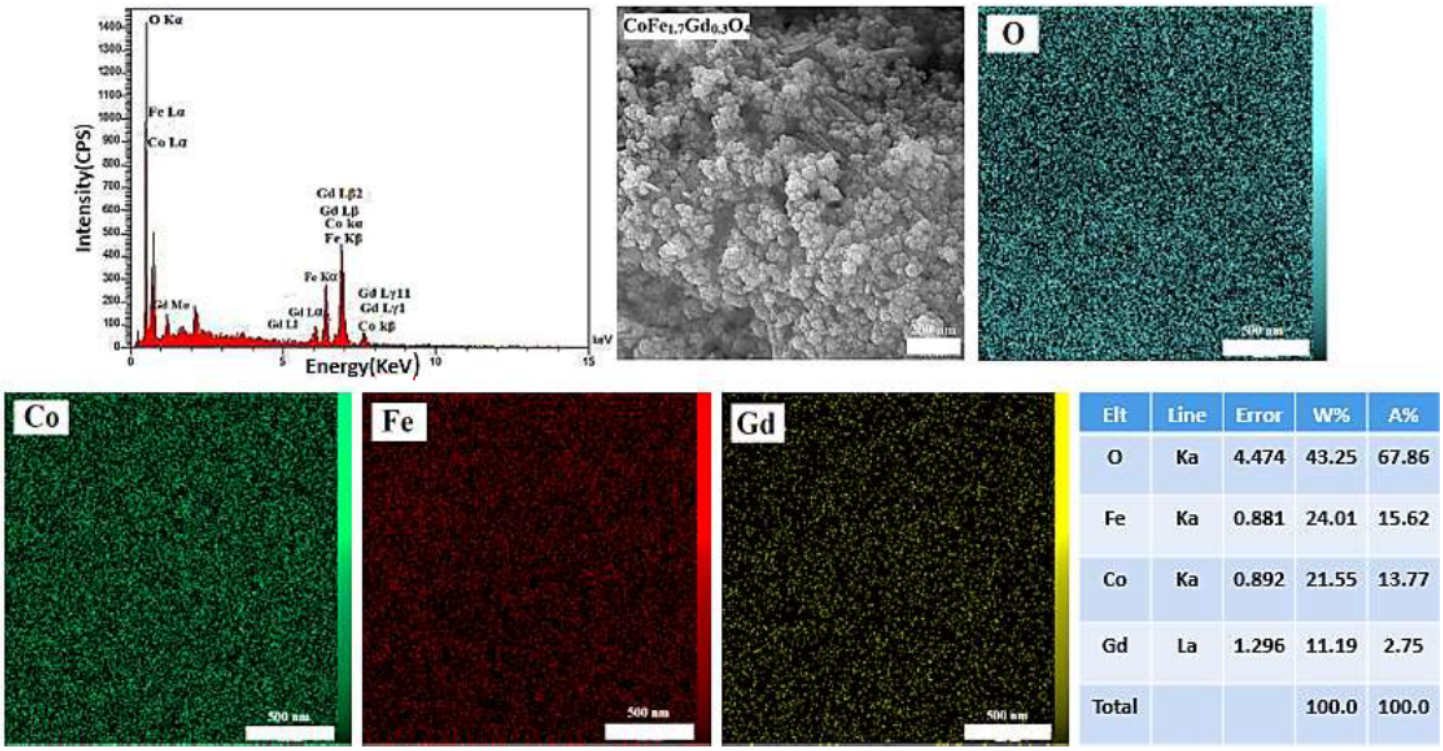

Elt	Line	Error	W%	A%
O	Ka	4.474	43.25	67.86
Fe	Ka	0.881	24.01	15.62
Co	Ka	0.892	21.55	13.77
Gd	La	1.296	11.19	2.75
Total			100.0	100.0

Figure 6

FESEM image, EDS pattern, and elemental map of $CFNG_{0.30}$ magnetic nanoparticles

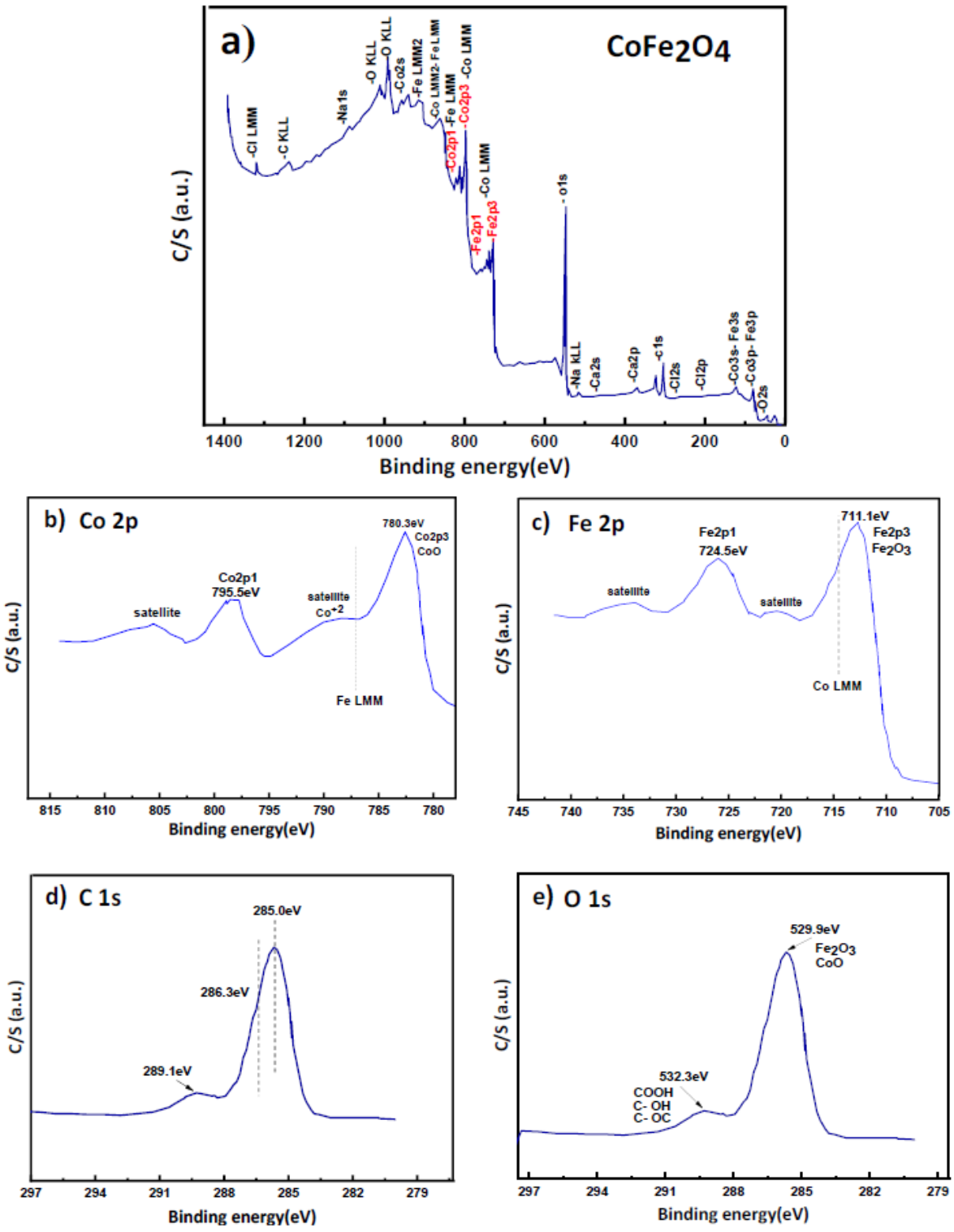

Figure 7

XPS spectrum of CFN 4 nanoparticles

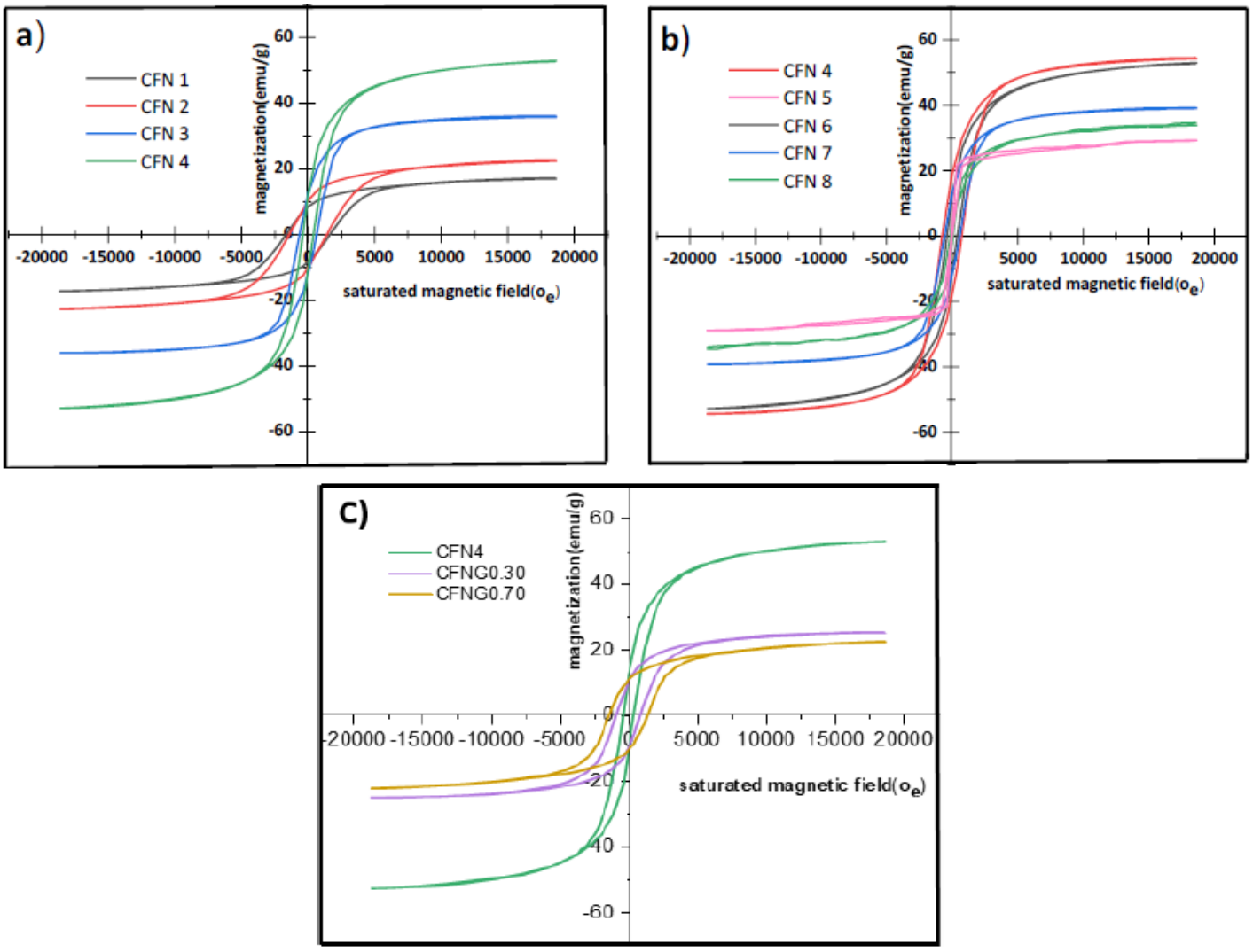

Figure 8

Effect of synthesis temperature (a), combination ratio (b), and Gd dopant (c) on the magnetization of $CoFe_2O_4$ nanoparticles